A First-Principles Approach for Treating Dye Wastewater

Adriano Santana, Andreia S. F. Farinha, Aniela Zarzar Toraño, Mahmoud Ibrahim, and Himanshu Mishra*

Water Desalination and Reuse Center (WDRC), Division of Biological and Environmental Science and Engineering (BESE), King Abdullah University of Science and Technology (KAUST), Thuwal 23955-6900, Saudi Arabia

*Corresponding author email: himanshu.mishra@kaust.edu.sa

1   **Abstract**

2

3   Numerous materials are employed for treating wastewaters, e.g., for the removal of dyes from wastewater

4   in the textile industry. However, the regeneration/reuse of these materials is still seldom practiced.

5   Quantitative insights into intermolecular forces between the contaminants and the functional surfaces

6   might aid the rational design of reusable materials. Here, we compare the efficacies of aliphatic (C_8H_{18}),

7   aromatic (C_6H_6), and aromatic perfluorinated (C_6F_6) moieties at removing methylene blue (MB^+),

8   as a surrogate dye, from water. We employed DFT with an implicit polarizable continuum model (PCM)

9   for water to accurately determine the contributions of the solvent's electrostatics in the adsorption process.

10   Our calculations pinpointed the relative contributions of π-π stacking, van der Waals complexation,

11   hydrogen bonding, and cation-π interactions, predicting that MB^+ would bind the strongest with C_6F_6

12   due to hydrogen bonding and the weakest with C_8H_{18}. Complementrary laboratory experiments

13   revealed that despite the similar hydrophobicity of silica beads functionalized with Si-C_8H_{17},

14   Si-C_6H_5, and Si-C_6F_5, as characterized by their water contact angles, the relative uptake of

15   aqueous MB^+ varied as Si-C_6F_5 (95%) > Si-C_6H_5 (35%) > Si-C_8H_{17} (3%). This first-principles-

16   led experimental approach can be easily extended to other classes of dyes, thereby advancing

17   the rational design of adsorbents.

18

1. INTRODUCTION

19

20   Domestic and industrial consumption of water has been increasing to meet the needs of growing
21   populations and industries around the world[1]. Water resources are therefore under tremendous stress to
22   cope with the demand for irrigated and livestock agriculture, as well as the industrial needs and the impact
23   of climate change and widespread contamination of land and water bodies[2-4]. In this context, wastewater
24   treatment serves the crucial purpose of water reuse and sustainable discharge into the environment[5]. The
25   recovery of materials and resources during wastewater treatment is also emerging as a promising approach
26   towards a circular-economy[6-9]. Treatment methods for wastewaters depend on their source and
27   contaminants, such as the removal of oil from produced water[10], the remediation of municipal waste with
28   microorganisms[11], or the treatment of textile effluents with macromolecular dyes[12]. Of these, we are
29   interested in the removal of dyes from wastewaters generated in industries, such as textile, cosmetics,
30   pulp and paper, food and beverages, packaging, paints, and pharmaceuticals[12]. Over 100,000
31   commercial dyes are known presently[13], with an annual consumption of $> 7 \times 10^8$ kg/yr[14]. About 5-
32   10% of these dyes appear in the effluent streams of industrial wastewater and are discharged into
33   oceans, rivers, and soils[12, 15]. Many of these dyes are potentially toxic and could pose a threat to the
34   environment[12, 13]. In response, traditional methods to remove dyes from wastewater include
35   adsorption, ion-exchange, oxidation, and coagulation/flocculation[16]. Adsorption is the most
36   common strategy due to its low cost, efficiency, and ease of operation[12]. Common "broad-spectrum"
37   adsorbents for dyes include activated carbon, silica gels, fly ash, bentonite, and perlite[12].
38   However, these adsorbents are not regenerated after usage and are subsequently disposed of as
39   waste[13]. The design of materials for adsorption has largely been empirical and without consideration
40   into intermolecular forces. Thus, there is a need for rationally designed reusable adsorbents for the
41   removal of macromolecular dyes from wastewaters.

42   The rational design of reusable adsorbent requires a quantitative understanding of the intermolecular
43   and surface forces between the target contaminants and the functional material used for removal of the
44   contaminants, such as ion-π interactions[17], π-π stacking[18], hydrogen bonding[19], and van der Waals
45   interactions[20], etc.[21] Reusable adsorbents should bind/physisorb to contaminants with energies in
46   the range of 5-10 $k_b T$/mol (3-6 kcal-mol^{-1}), which is not only strong enough to bind but
47   also weak enough to facilitate regeneration[21-24]. We chose methylene blue (MB) as a surrogate
48   dye in our model system because it is employed as a colorant in the paper and pulp industry[25] and
49   its low-cost and easy availability (Figure 1A). As an adsorbate, MB is quite "versatile": it can form
50   hydrogen bonds (H-bond) with electronegative atoms such as O, N, and F, it can accept electrons in

51   π-π stacks, it can participate in cation-π interations[17, 26] due to its cationic nature (Figure 1B), and

52   it can also interact through van der Waals interactions[27]. MB has been produced at mass-scale since

53   the late 19th century and it also serves a starting material for numerous azine dyes[25]. Its molecular

54   versatility is further evidenced by its medical use to treat depression[28], breast cancer[29], malaria[30],

55   Alzheimer's[31], and aging of the skin[32]. Yet, quantitative insights into the factors and mechanisms

56   governing the adsorption of MB even onto simple surfaces remain unclear. For example, it has been

57   suggested that dispersion interactions and hydrophobic interactions are important in the adsorption

58   of MB onto metals[27, 33] and silver iodide (AgI) suspensions[33], respectively, but a direct comparison

59   of those interactions remains unavailable. Here, we take an alternative approach towards rational

60   materials design – we utilize quantum mechanical calculations to gain insights into the nature of

61   binding and binding energies of a hydrated methylene blue cation (MB[+]) with a broad range of

62   aliphatic, aromatic and perfluorinated aromatics as surrogates for adsorbents (Figure 2).

63   Subsequently, we test these predictions through laboratory experiments using silica microspheres

64   terminated with the same aliphatic, aromatic, and perfluorinated aromatic groups. If successful, this

65   approach can be applied in principle to other dyes – anionic, cationic, zwitterionic, etc.

(A)   (B)
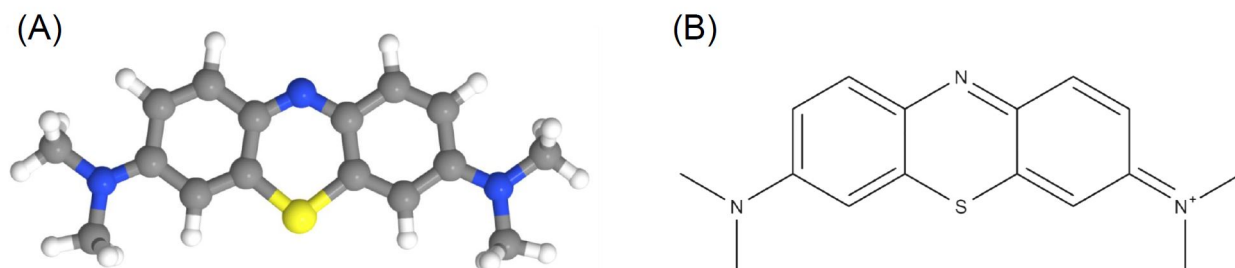

66

67   Figure 1: (A) A two-dimensional diagram of a methylene blue (MB) molecule. Color scheme:

68   Sulfur in yellow, nitrogen in dark blue, hydrogen in white, and carbon in grey. (B) The Lewis

69   structure of a methylene blue cation with the positive charge on a quaternary ammonium.

70

71   **MATERIALS AND METHODS**

72   **2.1. Quantum Mechanical Calculations**

73   DFT is a first-principles approach for predicting the electron density of a molecular/ionic

74   system, which employs a self-consistent field approach (SCF) for solving the Schrödinger

75   equation[34, 35]. It has been used extensively to perform electronic structure calculations in solid-state

76   physics and materials science[24, 36-39]. The accuracy of DFT in studying the electronic and physical

77   properties of materials is largely dependent on the choice of the exchange-correlation function. For

78   example, the local density approximation (LDA) and the generalized gradient approximation (GGA)

79   exchange-correlation functionals overestimate the dissociation energies and the hydrogen bonds,

80   respectively[38], and they require a dispersion energy correction when modeling van der Waals

81   interactions or studying water clusters[39]. Hybrid functionals such as B3LYP[40] provide a good

82   example of hydrogen bonding[41, 42], the structure of water clusters[43, 44], chemistries at the air-water

83   interface[45-48], graphene-based systems[49], guest-host binding of p-xylylenediamine to CB7[50],

84   vibrational spectra of hexafluorobenzene[51], and π-π interactions in dimers of benzene and

85   napthalene[18]. Thus, we considered B3LYP-level DFT to be suitable to investigate the molecular

86   interactions of MB^+ with hexafluorobenzene (C_6F_6), benzene (C_6H_6), and n-octane (C_8H_{18}) groups

87   (Figure 2). We account for the aqueous environment using the polarizable continuum model

88   (PCM)[52]. We chose these groups as surrogates for functional surfaces to gain insights into the vast

89   array of molecular interactions of MB^+ in an aqueous environment. We optimized numerous dimer

90   conformations using DFT implemented in the Gaussian software[53] at the B3LYP/6-311+G* level[40].

91   For the most difficult convergence cases due to the encounter of a shallow minima around the

92   stationary point, we employed the option *MaxStep* = 1 that led to full convergence. We subsequently

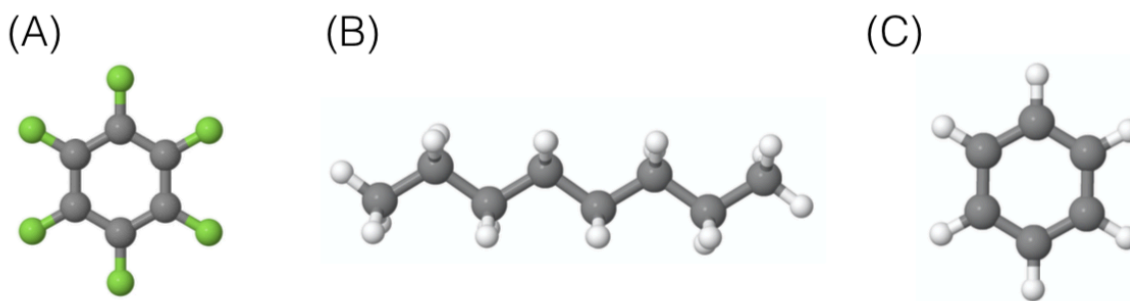93   confirmed the stability of the optimized structures through frequency calculations at each stationary

94   point.

95

96   Figure 2: Ball and stick diagrams of (A) hexafluorobenzene (C_6F_6), (B) octane (C_8H_{18}), and (C)

97   benzene (C_6H_6). Color scheme: carbon atoms (grey), fluorine (green) and hydrogen (white).

98

99   **2.2. Experimental: Synthesis of hollow silica microspheres.**

100   To test our computational predictions in the laboratory, we chose commercial silica microspheres,

101   3M™ Glass Bubbles[54], composed of soda-lime borosilicate glass with an average diameter ranging

102   16-65 μm (Figure S1A). We modified their surface chemistries through a two-step reaction of

103   hydroxylation, followed by silanation (Figure S1B).[55] To hydroxylate the silica surface, we

104 exposed the microspheres to an aqueous solution of hydrochloric acid (pH = 2) at 90 °C for one

105 hour (Section S1). Next, the surfaces were functionalized through silanation reactions with

106 triethoxy(octyl)silane, trimethoxyphenylsilane, and (pentafluorophenyl)triethoxysilane obtained

107 from Sigma-Aldrich (CAS: 2943-75-1, 2996-92-1, and 20083-34-5, respectively). Silanation

108 reactions were carried out in three batches, producing Si-C$_8$H$_{17}$, Si-C$_6$F$_5$, and Si-C$_6$H$_5$ (Section

109 S1)[56]. Obviously, we chose those silanes in accordance with our DFT calculations. MB was

110 obtained from Sigma-Aldrich (CAS: 122965-43-9) in the quaternary ammonium salt form

111 (C$_{16}$H$_{18}$ClN$_3$S·xH$_2$O, molecular 319.85 g/mol (anhydrous basis)). We incubated different amounts

112 of functionalized SiO$_2$ microspheres (0-100 mg) in aqueous solutions containing 100 ppm MB$^+$,

113 and repeated the experiment in quadruplicates (or higher). We mixed the solutions by gentle

114 tumbling for five minutes only, and a general scheme corresponding to the adsorption is

115 shown in Figure 3. Next, the SiO$_2$ microspheres floated up to the air-water interface due to their

116 lower density than water. We took aliquots of these solutions, diluted them with deionized

117 water, and characterized the concentrations of the remaining dye spectrophotometrically,

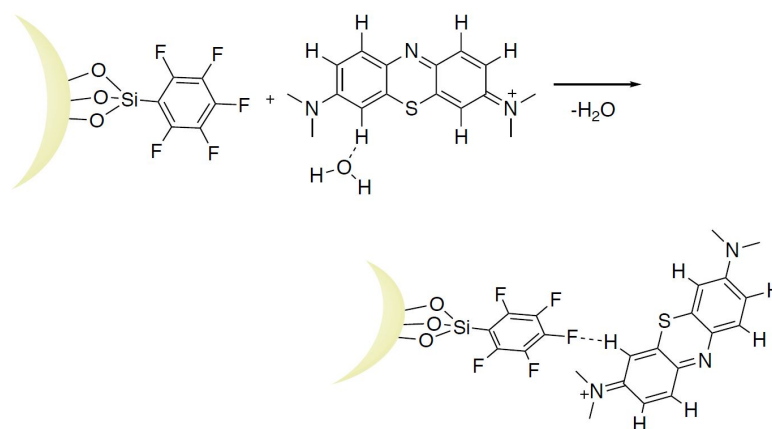118 using its extinction coefficient at 663 nm (Section S2).

119

120

121 Figure 3: A general scheme to show the adsorption of MB$^+$ onto functionalized silica beads: The

122 functionalized silica bead interacts with methylene blue in solution with one coordination water

123 molecule. Upon adsorption, the coordination water is released into the bulk and methylene blue

124 molecule interacts with the adsorbent.

125

126

127

6

128

3. Results and Discussion

3.1. Methylene blue in solution

Here we describe the state of the MB^+ cation in water. To begin, we calculate the molecular electrostatic potential (ESP) which is defined as the amount of work required to bring a positive unit charge from infinity to a distance r from the molecule[57, 58]. Thus, ESP comprises the contributions of the nuclear and the electronic charges, the latter calculated by methods such as Mulliken population analysis and Löwdin population analysis[59]. We obtained the ESP of MB^+ in water by mapping the electron density (chosen with a value of $\rho = 0.02$) onto the electrostatic potential[59]. The electron density was obtained from a Mulliken population analysis[57] of the optimized DFT structure of MB^+ in an aqueous environment, using the GaussView software (v. 5.0)[60] (Figure 4A). We found that hydrated MB^+ has a positive ESP due to the overall electron charge deficiency of the ion, with the hydrogen atoms being the most positive (blue color) due to their low electronegativity. Thus, MB^+ can potentially participate in hydrogen bonding through these H atoms by accepting electrons in π-π stacking, such as from benzene. The N and S atoms in the central ring (yellow color) behave neutrally towards electrophile/nucleophile molecules. The region between the C=C double bonds and the two tertiary nitrogen atoms also shows low electron densities (light blue color), albeit more than for the H atoms. We qualitatively infer from the ESP plot that MB^+ potentially participates in hydrogen bonding as well as π-π stacking and cation-π interactions.

3.2. Prediction of adsorption of MB^+

Here, we detail our semi-quantitative approach to predict the relative adsorption energies and rates of adsorption between MB^+ and our surrogate adsorbents. In order to make our model realistic, we added a water molecule in the coordination shell of MB^+ such that they had a binding energy of $E_{MB^+ \cdot H_2O}$. We chose that particular position of the water molecule, (Figure 3), because therein we obtained the strongest binding energy between the functional groups and MB^+. We assumed that this hydrogen bonded water needs to be removed from the coordination shell of MB^+, before it can adsorb onto silica beads and be removed from water. Figure 3 depicts this scheme with silica beads functionalized with C_6F_6. The released water molecule simply becomes a part of the bulk water, releasing a fixed amount of energy, E_{H_2O}, which is the equivalent of half of a water dimer. Next, we define the adsorption energy between MB^+ and the adsorbent as,

$$E_b = E_{dimer} - (E_{MB^+} + E_{adsb}) \ldots\ldots\ldots\ldots\ldots\ldots\ldots\ldots\ldots\ldots\ldots[1]$$

7

160 and

$$E_{ads} = E_b + E_{H_2O} - E_{MB^+ \cdot H_2O} \dots\dots\dots\dots\dots\dots\dots\dots\dots\dots[2]$$

162 where E_b is the binding energy of MB$^+$ and the adsorbent (after removing the explicit water

163 molecule), E_{dimer} is the electronic energy of the molecular complex (MB$^+$/adsorbent), E_{MB^+} is the

164 energy of a hydrated MB$^+$ cation, E_{adsb} is the energy of the adsorbent (one of the three stand-alone

165 surrogates), E_{ads} is the adsorption energy that we use to calculate binding constants, $E_{MB^+ \cdot H_2O}$ is the

166 energy of an MB$^+$.H$_2$O dimer in water. It should be noted that E_b refers to the energy holding MB$^+$-

167 adsorbent together whereas E_{ads} refers to the energy needed/released when displacing water from

168 the MB coordination shell to form the MB$^+$-adsorbent complex. We obtained a DFT binding energy

169 for a water dimer using the PCM model at 0 K of -5.4 kcal mol^{-1}. This is in good agreement with

170 the experimental value for the strength of the H-bond in a water dimer in a vacuum[61] of -5.58

171 kcal mol^{-1}, and also with previous theoretical calculations with the PCM model on the electron

172 energy of the water dimer[62] of -5.0 kcal mol^{-1}. Therefore, from our DFT-PCM calculations a

173 good estimate for E_{H_2O} is -2.7 kcal mol^{-1},[62] and with the same method we obtained a binding

174 energy for $E_{MB^+ \cdot H_2O}$ = -1.4 kcal mol^{-1} (Figure S4, Section S3). With these predicted adsorption

175 energies and assuming that in our dilute solutions only a single layer of MB$^+$ adsorbs onto the

176 functionalized surface, we used the Arrhenius equation to calculate the relative reaction rate

177 constants (k) by taking as a reference the reaction rate constant for the C$_8$ aliphatic, k_{ref}. We

178 assume that the pre-exponential factor, A, in the Arrhenius equation is the same in all three cases

179 and that the transition state barrier(s) that MB$^+$ has to overcome to bind to the surface are similar

180 in magnitude in all the cases. This assumption is reasonable because the molecular interactions

181 during the physisorption processes do not involve proton or electron transfers that would require

182 covalent bond breaking/forming and significant electrostatic preorganization.[63] Further, we

183 assume that thermal fluctuations (0.6 kcal mol^{-1}) facilitate MB$^+$, the solvent, and the surface to

184 sample through the configurational space to find the global minima. Thus, we can estimate the

185 relative binding rates as follows,

$$\frac{k}{k_{ref}} = e^{-(\Delta E_{ads})/k_b T} \dots\dots\dots\dots\dots\dots\dots\dots\dots\dots[3]$$

187 where $\boldsymbol{\Delta E_{ads}}$ is the adsorption energy as defined in equation 1 and relative to the adsorption energy

188 of the C$_8$ aliphatic. A simple rearrangement of equation 3 gives us the percentages of the relative

189 rates of adsorption as,

$$\frac{k - k_{ref}}{k_{ref}} \times 100 = (e^{-(\Delta E_{ads})/k_b T} - 1) \times 100 \dots\dots\dots\dots[4].$$

8

191

192 Next, we present the results of our DFT predictions for a variety of geometric confirmations between

193 MB^+ and C_6F_6, C_6H_6, and C_8H_{18} groups, with the aim of identifying the relative contributions of π-π

194 stacking, hydrogen bonding (H-bonding), cation-π interactions, and van der Waals forces to the

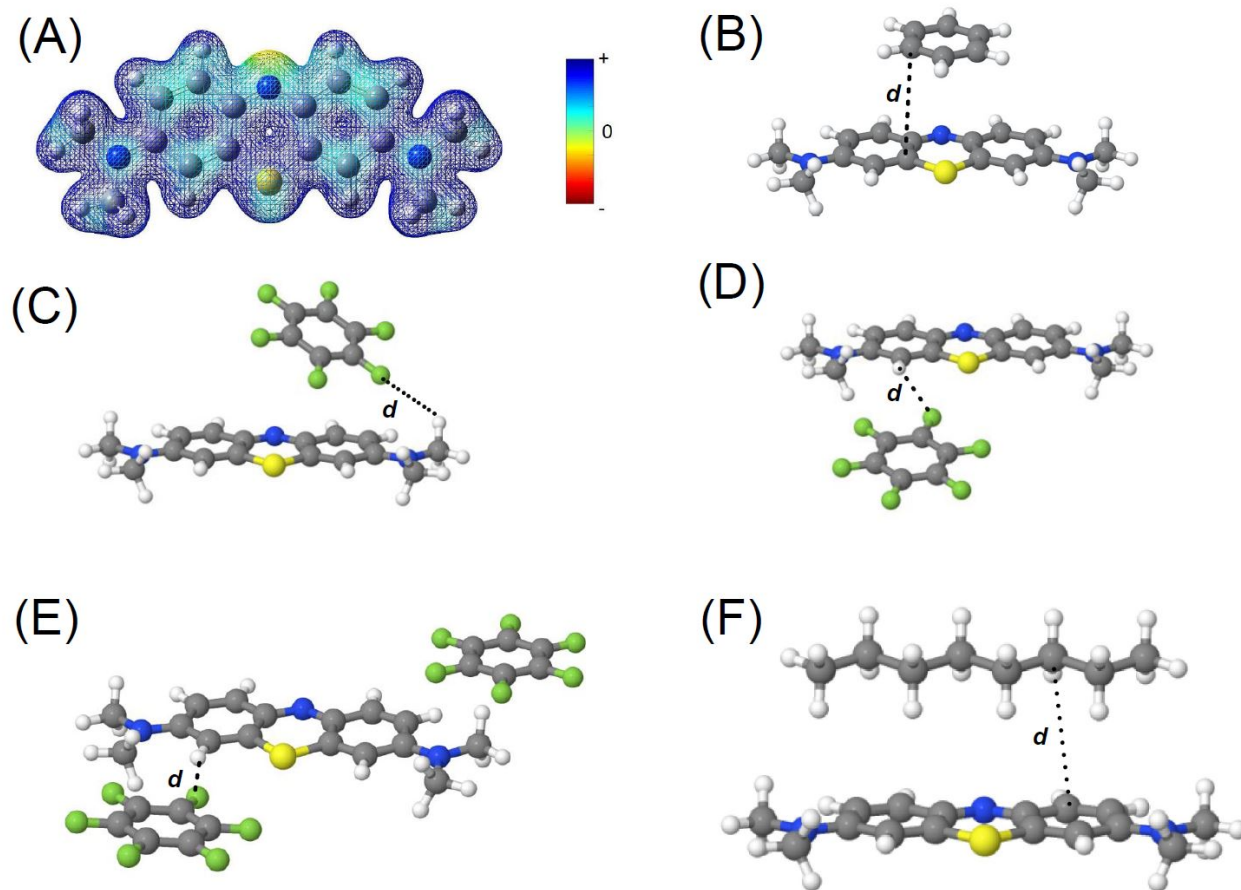195 adsorption process (Table 1).

196

197

198 Figure 4: (A) The electron density mapped with the electrostatic potential for a hydrated MB^+ cation.

199 For the plotted density, $\rho = 0.02$, the units range from (-0.27, 0.27) atomic units (a.u.). Regions with

200 positive ESP (blue) have lower electron density than the regions with negative ESP (red). The most

201 positive value in the ESP corresponds to the two hydrogen atoms next to the sulfur atom (yellow

202 color). The hydrated MB^+ cation is electron deficient, with the hydrogen atoms and the aromatic

203 rings having the lowest electron density. Snapshots from DFT calculations of (B) a MB^+-benzene

204 dimer in π-π stacking; (C), (D),(E) dimers between MB^+ and C_6F_6 featuring H-bonds; (F) MB^+-

205 C_8H_{18} dimer held by van der Waals interactions. Color scheme: fluorine green, hydrogen white,

206 carbon dark grey, sulfur yellow, and nitrogen dark blue.

207

3.3. π-π stacking between MB$^+$ and C$_6$H$_6$ and C$_6$F$_6$ groups

208

209   Benzene can donate electrons through its p_z orbital to MB$^+$ in water. In fact, we found that the dimer

210   MB$^+$-C$_6$H$_6$ has a stable configuration in the π-π stacking conformation (Figure 4B). The optimized

211   structure has an average intermolecular distance, d = 4.8 Å, between (C--C) indicating a weakly

212   bound dimer. This result is in overall agreement with higher-level electronic structure methods

213   such as MP2 and CCSD(T) for π-π sandwich benzene dimer which show an average

214   intermolecular distance, d=3.8-4.1 Å[64]. We found that the adsorption energy was E_{ads} = -2.9 kcal-

215   mol^{-1} (Table 1). Next, we substituted hydrogen atoms of benzene with fluorine atoms to simulate

216   interactions of MB$^+$ with C$_6$F$_6$. Fluorine has a deactivating effect on cation-π interactions[17, 65]

217   because electrons in C-F bonds are polarized towards fluorine atoms due to the latter's higher

218   electronegativity[66]. Thus, C$_6$F$_6$ is unlikely to interact with MB$^+$ through its π orbitals [26]. Thus, we

219   expected π-π stacking for the MB$^+$-C$_6$F$_6$ complex to be weaker than for the MB$^+$-C$_6$H$_6$ complex.

220   Indeed, we verified this to be true – while we arranged C$_6$F$_6$ to interact with MB$^+$ through

221   π-π stacking, (Figure 4B) the C$_6$F$_6$ molecule tilted over the MB$^+$ during geometry optimization and

222   underwent a significant displacement. The final structure comprised an MB$^+$-C$_6$F$_6$ complex with

223   hydrogen bonding between a fluorine atom and a hydrogen atom of MB$^+$ (Figure 4C). The shortest

224   distance between those atoms was, d = 3.1 Å and the adsorption energy was E_{ads} = -2.9 kcal mol^{-1}.

225

226 Table 1: Predictions of adsorption energies, E_{ads}, for π-π stacking, H-bonding, and van der Waals
227 interactions between MB$^+$ and C_6F_6, C_6H_6, and C_8H_{18} groups and the relative uptakes of MB$^+$ with
228 the performance of n-octane taken as the reference.

(Figure) Dimer	Key molecular interactions	Adsorption energy, E_{ads} (kcal-mol^{-1})	Predicted, relative uptake of MB$^+$(%) using equation [4]
(Fig. 4B) MB$^+$-C_6H_6	π-π stacking	-2.9	39%
(Fig. 4C) MB$^+$-C_6F_6	H-bond: F-H(methyl), sided	-2.9	39%
(Fig. 4D) MB$^+$-C_6F_6	H-bond: F-H(methyl)	-3.0	95%
(Fig. 4E) C_6F_6-MB$^+$-C_6F_6	H-bond: F-H(methyl)	-3.1	95%
(Fig. 4F) MB$^+$-C_8H_{18}	van der Waals	-2.7	0 (reference)

229

3.4. Hydrogen bonding

231 Since MB$^+$ and C_6F_6 interacted through H-bonding instead of π-π stacking, we investigated another
232 configuration whereby MB$^+$ and C_6F_6 were orientated facing each other. The final optimized
233 structure had two H-bonds – one between a fluorine atom and a hydrogen atom of a methyl group
234 of MB$^+$ and another between a fluorine atom and a hydrogen atom bound to an sp^2 carbon (Figure
235 4D). The shortest F-H distance was d =3.1 Å with the dimer adsorption energy, E_{ads} = -3.0 kcal
236 mol^{-1}. Surprisingly, although C_6F_6 can interact with MB$^+$ through π-π stacking, the overall low
237 electron density of MB$^+$ and the presence of fluorine favored the formation of H-bonds. It is
238 noteworthy that the adsorption energy also varied depending on the hybridization of the carbon
239 atom; C(sp^3)-F yielded a stronger hydrogen bond than C(sp^2)-F[67]. Interestingly, even a π-electron
240 donor like benzene yielded a lower E_{ads} = -2.9 kcal-mol^{-1} in comparison to H-bonded C_6H_6-MB$^+$
241 dimer with E_{ads} = -3.0 kcal mol^{-1}. To further confirm the importance of the H-bonding, we optimized
242 two C_6F_6 molecules with an MB$^+$ monomer. We found that, similar to the previous case, C_6F_6 made
243 H-bonds with MB$^+$ (Figure 4E). Fluorine atoms in C_6F_6 groups formed H-bonds with the methyl
244 groups in MB$^+$ but the shortest H-bond distance was to the hydrogen next to the sulfur atom, d = 2.8
245 Å and E_{ads} = -3.1 kcal mol^{-1} (Figure 4E). The adsorption energy was slightly more than that of
246 MB$^+$-C_6F_6, (Figure 4D), indicating that increasing the number of C_6F_6 species near MB$^+$ enhances
247 stabilization. However, when we studied the E_{ads} of MB$^+$.2(C_6H_6) in π-π stacking conformation

11

248   we did not find any increment in the adsorption energy. (Figure S5, Section S3). Thus, only in the

249   fluorinated case we found that the most stable configuration was that with ratio 2:1. The study of

250   3:1 or higher configurations were computationally unfeasible or unable to converge.

251

3.5. Cation-π interactions

253   MB^+ is a large cation that could potentially interact with a π-system. In the gas-phase, fluoro-

254   aromatic compounds are known to exhibit high binding energy with cations, e.g., the ab-initio

255   binding energy fluorobenzene with a lithium ion is, E_b = -31 kcal.mol^{-1}.[68] However, for MB^+

256   interacting with C_6F_6 in an aqueous environment, we did not find dimer configurations stabilized by

257   cation-π interactions (Figure S6, Section S3). The final optimized structures between MB^+ and C_6F_6

258   comprised H-bonds between F and H atoms similar to (Figure 4B), with similar binding energy and

259   H-bond distances. Thus, C_6F_6-MB^+ dimers optimized from the initial configurations of π-π stacking

260   or cation-π stacking were not stable, and the optimized structures always led to dimers interacting

261   by H-bonding. Furthermore, C_6H_6-MB^+ did not demonstrate configurations stabilized by cation-π

262   interactions or hydrogen bonding (only π-π stacking).

263

3.6. Van der Waals interactions

265   Finally, we investigated the interactions between the aliphatic chain C_8H_{18} and MB^+ in an aqueous

266   solution. We found that E_{ads} = -2.7 kcal mol^{-1}, and the interaction was driven by van der Waals

267   dispersion forces[27]. The average intermolecular distance, d = 3.2 Å (Figure 4F).

268

3.7.   A comparison of various intermolecular forces

270   Based on the predictions from QM, we listed the E_{ads} values due to different molecular

271   interactions in Table 1. We used equation [4] to predict the trend in the binding constants of the

272   three functional groups, C_6F_6 (H-bonding) > C_6H_6 (π-π stacking and H-bonding) > C_8H_{18} (vdW

273   dispersion). To gain quantitative insights, we benchmarked the binding constants against the

274   aliphatic group (C_8H_{18}) and found the relative adsorption to vary such that C_6F_6 (95%) > C_6H_6

275   (39%) > C_8H_{18} (0), which was an unexpected result. Next, we tested our predictions through

276   laboratory experiments.

277

278

279

| 280	### 3.8. Experimental adsorption of MB$^+$ on an organic substrate
281	We tested our theoretical prediction that H-bonding between MB$^+$ and C$_6$F$_6$ leads to a
282	dramatically higher adsorption than MB$^+$ and C$_6$H$_6$ due to π-π stacking or MB$^+$ and C$_8$F$_{18}$ due to
283	van der Waals dispersion. To this end, we measured the adsorption of MB$^+$ onto hollow silica
284	microspheres functionalized with -C$_8$H$_{17}$, -C$_6$H$_5$ and -C$_6$F$_5$ moieties (Methods Section 2.2). We
285	employed Attenuated total reflectance-Fourier transform infrared (ATR-FTIR) spectroscopy to
286	characterize the silica before and after functionalization (Figure S2). We found functional groups
287	Si-C$_8$H$_{17}$: asymmetric and symmetric CH$_2$ vibrations around 2922 cm^{-1} and 2852 cm^{-1} respectively;
288	Si-C$_6$F$_5$: C=C and C−F aromatic stretching bands at 1424 cm^{-1}; Si-C$_6$H$_5$: C-H stretch bands at
289	3074 cm^{-1} and 3052 cm^{-1} and C-C stretch (in-ring) at 1624 cm^{-1} and 1434 cm^{-1} (Section S1.2). We
290	note that the contact angles of water drops on glass slides functionalized with -C$_6$F$_5$, -C$_6$H$_5$, and
291	-C$_8$H$_{17}$ groups were similar after silanation, which led us to expect that their uptake of MB$^+$ might
292	be similar in magnitude (Section S1.3, Figure S3, and Table S1). This expectation was based on
293	the extant literature on the adsorption of simple and complex organics onto hydrophobic surfaces
294	in water - organic fouling – a leading cause for the failure of membrane-based separation
295	technologies[55, 69-72]. We also note that ξ-potentials of hydrocarbon and perfluorocarbon surfaces,
296	which have been investigated extensively in the past and intensely debated on regarding their
297	correlation with interfacial charges, could have a bearing on physisorption.[44, 73-75] However, due
298	to the hollowness of the beads, it was not possible to measure ξ-potentials of our specific samples
299	because they would not stay inside a water-filled cuvette. To measure the uptakes of MB$^+$ by silica
300	beads with different surface functionalization, the UV-VIS absorbance spectra of 100 ppm aqueous
301	solutions of MB$^+$, which follows the Lambert-Beer law, was measured. We found that the uptake of
302	MB$^+$ by our functionalized silica microspheres varied as: Si-C$_6$H$_5$ (95% $\pm$ 1.8%) > Si-C$_6$H$_5$
303	(35% $\pm$ 1.9%) > Si-C$_8$H$_{17}$ (3% $\pm$ 2.5%) (Figure 5). Thus, the alkyl derivative Si-C$_8$H$_{17}$ barely
304	adsorbed any MB$^+$, the perfluorinated benzene performed the best, and the benzene-terminated
305	microspheres performed intermediately, according to the predictions.
306	

307
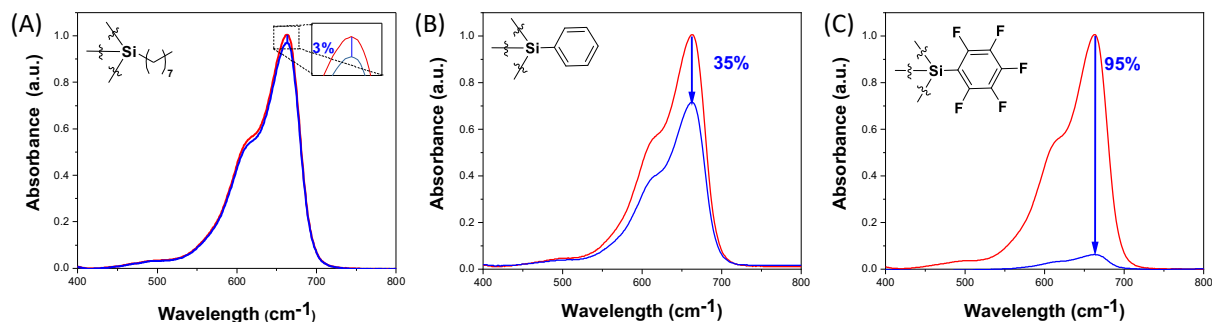
Figure 5: Absorbance spectra obtained after treating 20 mL MB^+ solutions (initial concentration: 100 ppm) with 100 mg of **A)** $Si\text{-}C_8H_{17}$, **B)** $Si\text{-}C_6H_5$, and **C)** $Si\text{-}C_6F_5$ adsorbent materials. MB^+ absorbance in the solution after mixing with functionalized silica beads decreased in the order $Si\text{-}C_6H_5$ (95% $\pm$ 1.8%) > $Si\text{-}C_6H_5$ (35%$\pm$ 1.9%) > $Si\text{-}C_8H_{17}$ (3%$\pm$ 2.5%). In all three cases the operational pH was 6.8.

We also performed the elemental analysis of the relative carbon contents of the functionalized silica beads, from the functional groups on the surfaces, and found no correlation between the amount of carbon and the extent of adsorption (see Section S1.4, Table S2). Thus, the dramatically different adsorption levels of MB^+ onto the functional groups were due to different intermolecular forces at play. After these experiments, the beads could be easily removed from the air-water interface as they floated up. We are currently developing greener methodologies for regenerating them that will be reported soon. Figure 6 summarizes this work.

The advantage of this approach relies on the calculation of relative electronic energies to study adsorption at solid-liquid interfaces. We have simplified the complex molecular representation of the functionalized (solid) surfaces by individual (functional) molecules. Of course, this approach has limitations, for instance, the use of free energies (thermal correction) instead of electronic energies at 0 K might be more accurate. However, since the adsorption energy is relatively proportional to the total electronic energy, the addition of the free energy contribution should not alter the predicted trends. Furthermore, the incorporation of vibrational frequencies into our energy calculations would be misleading because the individual (functional) molecules would behave more like a liquid, which in comparison to the solid phase, possesses extra rotational degrees of freedom. Despite these limitations, the model predictions are in

14

excellent agreement with experimental observations and should be extensible towards the development of rational treatment protocols for other wastewaters.
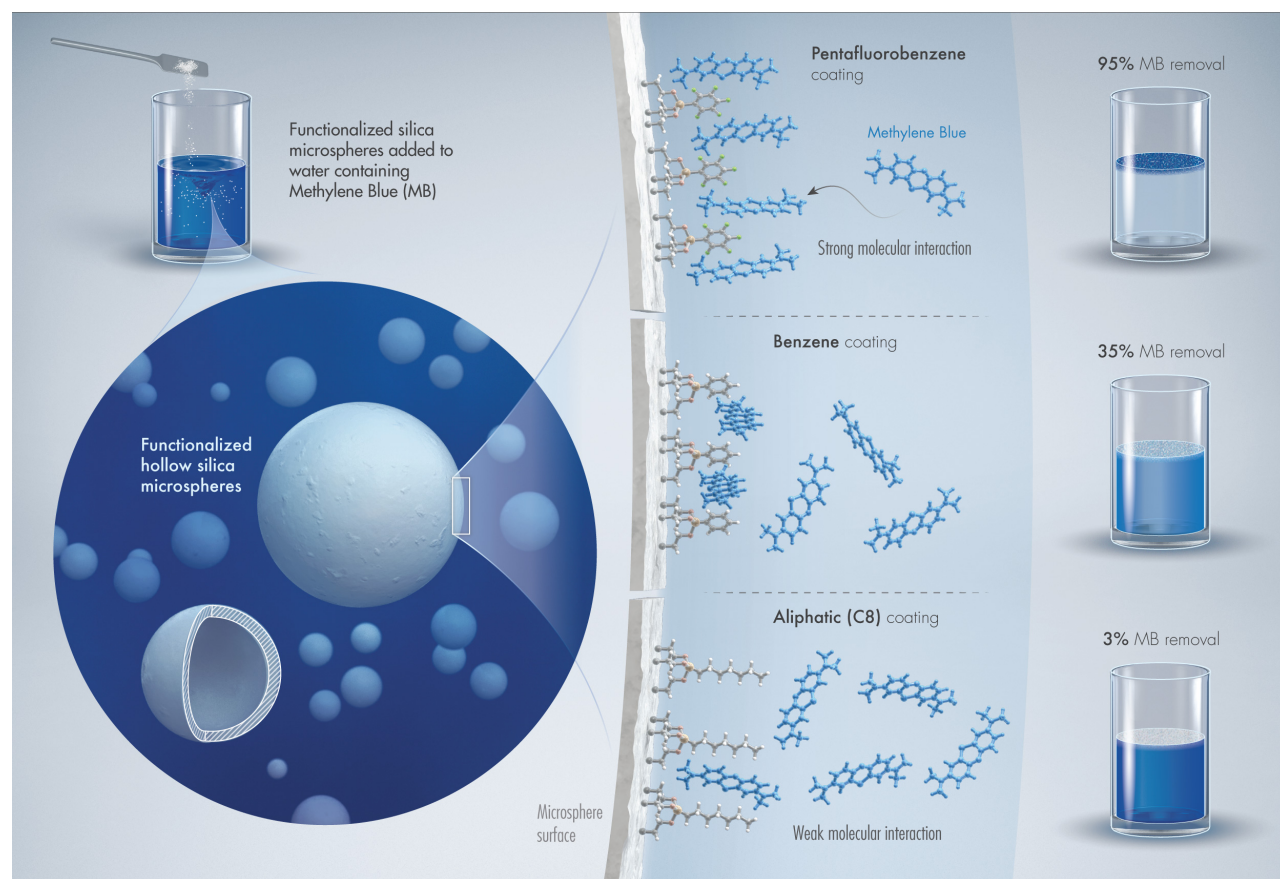

Figure 6: Schematics for our experimental work: (Left panel) hollow silica microspheres functionalized with $-C_6F_5$, $-C_6H_5$, $-C_8H_{17}$ were added to water with 100 ppm MB^+. (Middle panel) Intermolecular interactions between the silanized silica surfaces and MB^+ ions in water. (Right panel) The final outcome of our simulated water treatment experiments: pentafluorobenzene performed the best, followed by benzene, and the aliphatic group as, C_6F_5 (95% $\pm$ 1.8%) > Si-C_6H_5 (35%$\pm$ 1.9%) > Si-C_8H_{17}.

4. Conclusion

Towards rationally designing reusable adsorbents for chemically "versatile" dyes in wastewater streams from textile, cosmetics, pulp and paper, food and beverages, packaging, paints, and pharmaceutical industries, we investigated molecular interactions of MB^+, as a surrogate contaminant, with C_6F_6, C_6H_6, and C_8H_{18} groups as representative of functional surfaces. DFT was employed with an implicit water model (PCM) to accurately determine the contributions of the

15

349 solvent's electrostatics in the adsorption process. Model calculations predicted that the primary
350 intermolecular interactions of MB^+ with these functional groups are: hydrogen bonding between
351 MB^+ and C_6F_6; π-π stacking between C_6H_6 and MB^+ and van der Waals dispersion interactions
352 between C_8H_{18}-MB^+, such that the relative magnitudes of the binding constants varied as: C_6F_6
353 (95%) > C_6H_6 (39%) > C_8H_{18} (0). Thus, the model predicted that fluorinated aromatics are more
354 suitable for removing MB^+ from water than ordinary aromatics and hydrocarbons. Gaining these
355 molecular insights from an exclusively experimental approach would be very difficult. For instance,
356 one cannot predict the observed behaviors based on water contact angles, which are often used to
357 assess surfaces' ability to aggregate organics in water by hydrophobic interactions[76]. Thus, this report
358 illustrates that specific understanding of intermolecular forces is crucial in the case of complex dyes,
359 such as MB^+. Our laboratory experiments attest to the predicted trends for the relative uptakes of
360 MB^+ as: Si-C_6F_5 (95% $\pm$ 1.8%) > Si-C_6H_5 (35% $\pm$ 1.9%) > Si-C_8H_{17} (3% $\pm$ 2.5%). Here, we also
361 point out that the scope of this work is limited to presenting a first-principles computational approach
362 to the rational development of reusable adsorbents for treating dye wastewater. We chose methylene
363 blue – a cationic dye – simply to demonstrate the power of our quantum mechanical approach.
364 Obviously, the same approach can be extended to anionic, zwitterionic, or uncharged dyes to extend
365 the work to a broader and industrially relevant context, and also for finding greener and fouling-
366 resistant materials/approaches.[72, 77-80] We are currently investigating the specificity during the
367 adsorption process in the presence of multiple contaminants, and scenarios where the contaminants
368 in wastewater streams are concentrated, leading to the adsorption of multilayers. Taken together,
369 our findings suggest that this first-principles approach, supported by laboratory experiments, for the
370 rational design of functional materials in the treatment of wastewater can contribute to the sustainable
371 use of water.
372
373
374

REFERENCES

1. *(United Nations World Water Assessment Programme) Water and Energy (Volume 1). The United Nations World Water Development Report 2014*; United Nations: Paris, France, 2014; p 230.
2. FAO *The future of food and agriculture: Trends and challenges*; 2017.
3. Rodell, M.; Famiglietti, J.; Wiese, D.; Reager, J.; Beaudoing, H.; Landerer, F. W.; Lo, M.-H., Emerging trends in global freshwater availability. *Nature* **2018,** *557* (7707), 651.
4. Yutkin, M. P.; Mishra, H.; Patzek, T. W.; Lee, J.; Radke, C. J., Bulk and surface aqueous speciation of calcite: implications for low-salinity waterflooding of carbonate reservoirs. *SPE Journal* **2018**.
5. *(United Nations World Water Assessment Programme) The United Nations World Water Development Report 2018: Nature-based Solutions.*; Paris, UNESCO, 2018.
6. Angenent, L. T.; Karim, K.; Al-Dahhan, M. H.; Wrenn, B. A.; Domíguez-Espinosa, R., Production of bioenergy and biochemicals from industrial and agricultural wastewater. *Trends Biotechnol.* **2004,** *22* (9), 477-485.
7. *(United Nations World Water Assessment Programme) The United Nations World Water Development Report 2017. Wastewater: The Untapped Resource*; UNESCO: Paris, 2017.
8. Katuri, K. P.; Kalathil, S.; Ragab, A.; Bian, B.; Alqahtani, M. F.; Pant, D.; Saikaly, P. E., Dual-Function Electrocatalytic and Macroporous Hollow-Fiber Cathode for Converting Waste Streams to Valuable Resources Using Microbial Electrochemical Systems. *Adv. Mater.* **2018,** *30* (26), 1707072.
9. Stahel, W. R., The circular economy. *Nature* **2016,** *531* (7595), 435-438.
10. Jiménez, S.; Micó, M.; Arnaldos, M.; Medina, F.; Contreras, S., State of the art of produced water treatment. *Chemosphere* **2018,** *192*, 186-208.
11. Hong, P.-Y.; Julian, T.; Pype, M.-L.; Jiang, S.; Nelson, K.; Graham, D.; Pruden, A.; Manaia, C., Reusing treated wastewater: consideration of the safety aspects associated with antibiotic-resistant bacteria and antibiotic resistance genes. *Water* **2018,** *10* (3), 244.
12. Yagub, M. T.; Sen, T. K.; Afroze, S.; Ang, H. M., Dye and its removal from aqueous solution by adsorption: a review. *Adv. Colloid Interface Sci.* **2014,** *209*, 172-184.
13. Salahshoor, Z.; Shahbazi, A., Review of the use of mesoporous silicas for removing dye from textile wastewater. *Eur. J. Env. Sci.* **2014,** *4* (2).
14. Robinson, T.; McMullan, G.; Marchant, R.; Nigam, P., Remediation of dyes in textile effluent: a critical review on current treatment technologies with a proposed alternative. *Bioresour. Tech.* **2001,** *77* (3), 247-255.
15. Gürses, A.; Açıkyıldız, M.; Güneş, K.; Gürses, M. S., Dyes and pigments: their structure and properties. In *Dyes and Pigments*, Springer: 2016; pp 13-29.
16. Purkait, M. K.; Maiti, A.; Dasgupta, S.; De, S., Removal of congo red using activated carbon and its regeneration. *J. Hazard. Mater.* **2007,** *145* (1-2), 287-295.
17. Dougherty, D. A., The cation− π interaction. *Acc. Chem. Res.* **2012,** *46* (4), 885-893.
18. Sato, T.; Tsuneda, T.; Hirao, K., A density-functional study on π-aromatic interaction: Benzene dimer and naphthalene dimer. *J. Chem. Phys.* **2005,** *123* (10), 104307.
19. Israelachvili, J. N., Intermolecular and surface forces: revised third edition. Academic press Waltham, MA: 2011.
20. Bera, B.; Shahidzadeh, N.; Mishra, H.; Belyaeva, L. A.; Schneider, G. F.; Bonn, D., Wetting of water on graphene nanopowders of different thicknesses. *Appl. Phys. Lett.* **2018,** *112* (15), 151606.
21. Whitten, K.; Davis, R.; Larry Peck, M., *General Chemistry (Pg 486, Table 13-3)*. 7 ed.; Cengage Learning: 2003; p 1224.
22. Lackner, K. S., The thermodynamics of direct air capture of carbon dioxide. *Energy* **2013,** *50*, 38-46.
23. Mishra, H.; Yu, C.; Chen, D. P.; Goddard III, W. A.; Dalleska, N. F.; Hoffmann, M. R.; Diallo, M. S., Branched polymeric media: boron-chelating resins from hyperbranched polyethylenimine. *Environ. Sci. Technol.* **2012,** *46* (16), 8998-9004.

425   24.   Mendoza-Cortés, J. L.; Han, S. S.; Furukawa, H.; Yaghi, O. M.; Goddard III, W. A., Adsorption
426 mechanism and uptake of methane in covalent organic frameworks: theory and experiment. *J. Phys.*
427 *Chem. A* **2010,** *114* (40), 10824-10833.
428   25.   Kalra, A.; Garde, S.; Hummer, G., Osmotic water transport through carbon nanotube
429 membranes. *P Natl Acad Sci USA* **2003,** *100* (18), 10175-10180.
430   26.   Gallivan, J. P.; Dougherty, D. A., Can Lone Pairs Bind to a π System? The Water---
431 Hexafluorobenzene Interaction. *Org. Lett.* **1999,** *1* (1), 103-106.
432   27.   Zhou, L.; Johnson, R.; Habteyes, T.; Guo, H., Adsorption of methylene blue and its N-
433 demethylated derivatives on the (111) face of coinage metals: The importance of dispersion
434 interactions. *J. Chem. Phys.* **2017,** *146* (16), 164701.
435   28.   Delport, A.; Harvey, B. H.; Petzer, A.; Petzer, J. P., Methylene blue and its analogues as
436 antidepressant compounds. *Metab. Brain Disease* **2017,** *32* (5), 1357-1382.
437   29.   dos Santos, A. F.; Terra, L. F.; Wailemann, R. A.; Oliveira, T. C.; de Morais Gomes, V.; Mineiro,
438 M. F.; Meotti, F. C.; Bruni-Cardoso, A.; Baptista, M. S.; Labriola, L., Methylene blue photodynamic
439 therapy induces selective and massive cell death in human breast cancer cells. *BMC cancer* **2017,** *17*
440 (1), 194.
441   30.   Meissner, P. E.; Mandi, G.; Coulibaly, B.; Witte, S.; Tapsoba, T.; Mansmann, U.;
442 Rengelshausen, J.; Schiek, W.; Jahn, A.; Walter-Sack, I., Methylene blue for malaria in Africa: results
443 from a dose-finding study in combination with chloroquine. *Malar. J.* **2006,** *5* (1), 84.
444   31.   Atamna, H.; Kumar, R., Protective role of methylene blue in Alzheimer's disease via
445 mitochondria and cytochrome c oxidase. *J. Alzheimer's Dis.* **2010,** *20* (s2), S439-S452.
446   32.   Xiong, Z.-M.; O'Donovan, M.; Sun, L.; Choi, J. Y.; Ren, M.; Cao, K., Anti-aging potentials of
447 methylene blue for human skin longevity. *Sci. Rep.* **2017,** *7* (1), 2475.
448   33.   De Keizer, A.; Fokkink, L., Specific adsorption of organic cations at the silver iodide—
449 electrolyte interface. *Colloids Surf. A* **1990,** *51*, 323-337.
450   34.   Pople, J. A.; Gill, P. M.; Handy, N. C., Spin-unrestricted character of Kohn-Sham orbitals for
451 open-shell systems. *Int. J. Quantum Chem.* **1995,** *56* (4), 303-305.
452   35.   Kohn, W.; Sham, L. J., Self-consistent equations including exchange and correlation effects.
453 *Phys. Rev.* **1965,** *140* (4A), A1133.
454   36.   Koch, W.; Holthausen, M. C., *A chemist's guide to density functional theory*. John Wiley & Sons:
455 2015.
456   37.   Grimme, S.; Antony, J.; Schwabe, T.; Mück-Lichtenfeld, C., Density functional theory with
457 dispersion corrections for supramolecular structures, aggregates, and complexes of (bio) organic
458 molecules. *Org. Biomol. Chem.* **2007,** *5* (5), 741-758.
459   38.   Pérez-Jordá, J. M.; Becke, A. D., A density-functional study of van der Waals forces: rare gas
460 diatomics. *Chemical Physics Letters* **1995,** *233* (1-2), 134-137.
461   39.   Grimme, S.; Antony, J.; Ehrlich, S.; Krieg, H., A consistent and accurate ab initio
462 parametrization of density functional dispersion correction (DFT-D) for the 94 elements H-Pu. *J.*
463 *Chem. Phys.* **2010,** *132* (15), 154104.
464   40.   Becke, A., Density-functional thermochemistry: The role of extract exchange. *J. Chem. Phys.*
465 **1993,** *98* (5), 648-5.
466   41.   Plumley, J. A.; Dannenberg, J., A comparison of the behavior of functional/basis set
467 combinations for hydrogen-bonding in the water dimer with emphasis on basis set superposition
468 error. *J. Comp. Chem.* **2011,** *32* (8), 1519-1527.
469   42.   Chen, Y.-f.; Dannenberg, J., Cooperative 4-pyridone H-bonds with extraordinary stability. A
470 DFT molecular orbital study. *J. Am. Chem. Soc.* **2006,** *128* (25), 8100-8101.
471   43.   Bryantsev, V. S.; Diallo, M. S.; Van Duin, A. C.; Goddard III, W. A., Evaluation of B3LYP, X3LYP,
472 and M06-class density functionals for predicting the binding energies of neutral, protonated, and
473 deprotonated water clusters. *J. Chem. Theory Comput.* **2009,** *5* (4), 1016-1026.
474   44.   Mishra, H.; Enami, S.; Nielsen, R. J.; Stewart, L. A.; Hoffmann, M. R.; Goddard, W. A.; Colussi, A.
475 J., Brønsted basicity of the air–water interface. *Proc. Natl. Acad. Sci. U.S.A.* **2012,** *109* (46), 18679-
476 18683.

477 45.   Mishra, H.; Nielsen, R. J.; Enami, S.; Hoffmann, M. R.; Colussi, A. J.; Goddard, W. A., Quantum
478 chemical insights into the dissociation of nitric acid on the surface of aqueous electrolytes. *Int. J.*
479 *Quantum Chem.* **2013,** *113* (4), 413-417.
480 46.   Mishra, H.; Enami, S.; Nielsen, R. J.; Hoffmann, M. R.; Goddard, W. A.; Colussi, A. J., Anions
481 dramatically enhance proton transfer through aqueous interfaces. *P Natl Acad Sci USA* **2012,** *109* (26),
482 10228-10232.
483 47.   Gallo, A.; Farinha, A. S.; Dinis, M.; Emwas, A.-H.; Santana, A.; Nielsen, R. J.; Goddard, W. A.;
484 Mishra, H., The chemical reactions in electrosprays of water do not always correspond to those at the
485 pristine air–water interface. *Chem. Sci.* **2019,** *10* (9), 2566-2577.
486 48.   Colussi, A. J.; Enami, S.; Yabushita, A.; Hoffmann, M. R.; Liu, W.-G.; Mishra, H.; Goddard III, W.
487 A., Tropospheric aerosol as a reactive intermediate. *Faraday Discuss.* **2013,** *165*, 407-420.
488 49.   Shi, H.; Auerbach, S. M.; Ramasubramaniam, A., First-principles predictions of structure–
489 function relationships of graphene-supported platinum nanoclusters. *J. Phys. Chem. C* **2016,** *120* (22),
490 11899-11909.
491 50.   Jensen, J. H., Predicting accurate absolute binding energies in aqueous solution:
492 thermodynamic considerations for electronic structure methods. *Phys. Chem. Chem. Phys.* **2015,** *17*
493 (19), 12441-12451.
494 51.   Rajaa, G.; Saravananb, K.; Sivakumarc, S., Analysis on vibrational spectra of
495 Hexafluorobenzene based on density functional theory calculations. **2011**.
496 52.   Tomasi, J.; Mennucci, B.; Cammi, R., Quantum mechanical continuum solvation models. *Chem.*
497 *Rev.* **2005,** *105* (8), 2999-3094.
498 53.   Frisch, M.; Trucks, G.; Schlegel, H. B.; Scuseria, G.; Robb, M.; Cheeseman, J.; Scalmani, G.;
499 Barone, V.; Mennucci, B.; Petersson, G., Gaussian 09, revision a. 02, gaussian. *Inc., Wallingford, CT*
500 **2009,** *200*, 28.
501 54.   Lingk, O. 3M Glass Bubbles: Lightweight Compounds and Composites based on High Strength
502 Hollow Glass Microspheres. https://www.b2match.eu/system/nl-
503 nrw2016/files/3M_Germany.pdf?1456150121.
504 55.   Subramanian, N.; Qamar, A.; Alsaadi, A.; Gallo, A.; Ridwan, M. G.; Lee, J.-G.; Pillai, S.;
505 Arunachalam, S.; Anjum, D.; Sharipov, F.; Ghaffour, N.; Mishra, H., Evaluating the potential of
506 superhydrophobic nanoporous alumina membranes for direct contact membrane distillation. *Journal*
507 *of Colloid and Interface Science* **2019,** *533*, 723-732.
508 56.   Mishra, H.; Farinha, A. S.; Sinha, S. Functionalized SiO2 microspheres for extracting oil from
509 produced water. 2016.
510 57.   Andrew, R. L., Molecular modeling principles and applications. *2nd, editor.: Pearson Education*
511 *Limited* **2001**.
512 58.   Murray, J. S.; Politzer, P., The electrostatic potential: an overview. *Wiley Interdisciplinary*
513 *Reviews: Computational Molecular Science* **2011,** *1* (2), 153-163.
514 59.   Jensen, F., *Introduction to computational chemistry*. John wiley & sons: 2017.
515 60.   Dennington, R.; Keith, T.; Millam, J. G., GaussView version 5; Semichem Inc. *Shawnee Mission,*
516 *KS* **2009**.
517 61.   Suresh, S.; Naik, V., Hydrogen bond thermodynamic properties of water from dielectric
518 constant data. *J. Chem. Phys.* **2000,** *113* (21), 9727-9732.
519 62.   Feyereisen, M. W.; Feller, D.; Dixon, D. A., Hydrogen bond energy of the water dimer. *J. Phys.*
520 *Chem.* **1996,** *100* (8), 2993-2997.
521 63.   Kamerlin, S. C. L.; Warshel, A., At the dawn of the 21st century: Is dynamics the missing link for
522 understanding enzyme catalysis? *Proteins: Structure, Function, and Bioinformatics* **2010,** *78* (6), 1339-
523 1375.
524 64.   Sinnokrot, M. O.; Valeev, E. F.; Sherrill, C. D., Estimates of the ab initio limit for $\pi-\pi$
525 interactions: The benzene dimer. *J. Am. Chem. Soc.* **2002,** *124* (36), 10887-10893.
526 65.   Mecozzi, S.; West, A. P.; Dougherty, D. A., Cation$-\pi$ interactions in simple aromatics:
527 electrostatics provide a predictive tool. *J. Am. Chem. Soc.* **1996,** *118* (9), 2307-2308.

528 66.   Pauling, L., The nature of the chemical bond. IV. The energy of single bonds and the relative
529 electronegativity of atoms. *J. Am. Chem. Soc.* **1932,** *54* (9), 3570-3582.
530 67.   Howard, J. A.; Hoy, V. J.; O'Hagan, D.; Smith, G. T., How good is fluorine as a hydrogen bond
531 acceptor? *Tetrahedron* **1996,** *52* (38), 12613-12622.
532 68.   Razgulin, A. V.; Mecozzi, S., Binding properties of aromatic carbon-bound fluorine. *J. Med.*
533 *Chem.* **2006,** *49* (26), 7902-7906.
534 69.   Liu, C.; Chen, L.; Zhu, L., Fouling mechanism of hydrophobic polytetrafluoroethylene (PTFE)
535 membrane by differently charged organics during direct contact membrane distillation (DCMD)
536 process: An especial interest in the feed properties. *Journal of Membrane Science* **2018,** *548*, 125-135.
537 70.   Naidu, G.; Jeong, S.; Vigneswaran, S.; Hwang, T.-M.; Choi, Y.-J.; Kim, S.-H., A review on fouling
538 of membrane distillation. *Desalination and Water Treatment* **2016,** *57* (22), 10052-10076.
539 71.   Rezaei, M.; Warsinger, D. M.; Duke, M. C.; Matsuura, T.; Samhaber, W. M., Wetting phenomena
540 in membrane distillation: Mechanisms, reversal, and prevention. *Water research* **2018,** *139*, 329-352.
541 72.   Das, R.; Arunachalam, S.; Ahmad, Z.; Manalastas, E.; Mishra, H., Bio-inspired gas-entrapping
542 membranes (GEMs) derived from common water-wet materials for green desalination. *J. Membrane*
543 *Sci.* **2019**, 117185.
544 73.   Beattie, J. K., The intrinsic charge on hydrophobic microfluidic substrates. *Lab Chip* **2006,** *6*
545 (11), 1409-11.
546 74.   McCarty, L. S.; Whitesides, G. M., Electrostatic charging due to separation of ions at interfaces:
547 Contact electrification of ionic electrets. *Angew Chem Int Edit* **2008,** *47* (12), 2188-2207.
548 75.   Roger, K.; Cabane, B., Uncontaminated Hydrophobic/Water Interfaces Are Uncharged: A Reply.
549 *Angewandte Chemie International Edition* **2012,** *51* (52), 12943-12945.
550 76.   Lum, K.; Chandler, D.; Weeks, J. D., Hydrophobicity at small and large length scales. *J. Phys.*
551 *Chem. B* **1999,** *103* (22), 4570-4577.
552 77.   Domingues, E. M.; Arunachalam, S.; Nauruzbayeva, J.; Mishra, H., Biomimetic coating-free
553 surfaces for long-term entrapment of air under wetting liquids. *Nat. Commun.* **2018,** *9* (1), 3606.
554 78.   Domingues, E. M.; Arunachalam, S.; Mishra, H., Doubly reentrant cavities prevent catastrophic
555 wetting transitions on intrinsically wetting surfaces. *ACS Appl. Mater. Inter.* **2017,** *9* (25), 21532-
556 21538.
557 79.   Gonzalez-Avila, S. R.; Nguyen, D. M.; Arunachalam, S.; Domingues, E. M.; Mishra, H.; Ohl, C.-D.,
558 Mitigating cavitation erosion using biomimetic gas-entrapping microtextured surfaces (GEMS).
559 *Science Advances* **2020,** *6* (13), eaax6192.
560 80.   Pillai, S.; Santana, A.; Das, R.; Shrestha, B. R.; Manalastas, E.; Mishra, H., A molecular to macro
561 level assessment of direct contact membrane distillation for separating organics from water. *Journal*
562 *of Membrane Science* **2020,** *608*, 118140.
563

564

571

572

573 **Notes**

574 HM and ASSF have filed a US Patent application#US20180250656A1

575

576 **Funding Information**

578

579